



HEAT-EXCHANGE RELATIONS FOR UNGLAZED TRANSPIRED SOLAR COLLECTORS WITH CIRCULAR HOLES ON A SQUARE OR TRIANGULAR PITCH

G. W. E. VAN DECKER*, K. G. T. HOLLANDS**† and A. P. BRUNGER***

*RenewABILITY Energy Inc., P.O. Box 770301166 Bank St., Ottawa, ON K1S 5N2, Canada

**Department of Mechanical Engineering, University of Waterloo, Waterloo, ON N2L 3G1, Canada

***Bodycote Ortech Inc., 2395 Speakman Drive, Mississauga, ON, Canada

Received 11 May 2000; accepted 3 January 2001

Communicated by BRIAN NORTON

Abstract—The unglazed transpired solar collector is now an established solar air heater for heating outside air directly. Sample applications include pre-heating ventilation air and heating air for crop drying. The outside air in question is drawn straight from ambient, uniformly through the whole surface of a perforated blackened plate (the absorber plate) exposed to the sun. An important parameter in fixing the collector's efficiency is the heat exchange effectiveness, ϵ . Once ϵ is known, finding the collector's efficiency is straightforward. This paper presents measurements of ϵ for the case where the plate is perforated with circular holes on either a square or triangular layout, covering a range of wind speeds extending from zero to 5 m/s. These data extend the earlier measurements of Kutscher to a wider range of plate thicknesses, hole spacings (pitch), suction velocities, and to include a square layout of the holes. In the region where the two experiments overlap, agreement between the two is excellent. A new predictive model is developed that is based on breaking down the total heat transfer into contributions from each of the plate sections: the front, the hole and the back. Excellent agreement was found between modelled and measured ϵ ; the new measured data were predicted with a 4.2% root mean squared error (RMSE) and Kutscher's measured data is predicted within 6.3% RMSE. © 2001 Elsevier Science Ltd. All rights reserved.

1. INTRODUCTION

Unglazed, transpired solar collectors (Hollick and Peter, 1990; Kutscher *et al.*, 1991, 1993) have been the subject of a number of recent investigations (Gunnewiek *et al.*, 1997; Dymond and Kutscher, 1997; Arulanandam *et al.*, 2000). They are effective devices for applications where outside air is to be heated directly, such as in heating ventilation air for buildings and crop drying. The outside air in question is drawn straight from ambient, through the whole surface of a transpired, dark-coloured plate (the absorber plate), which has been perforated with holes, typically with a porosity of about 0.5%. Tests conducted on several installations indicate that the unglazed transpired collector (UTC) works very well with annual solar collection efficiencies reaching 72% (Carpenter and Kokko, 1991). Over 70 large systems, each having collector areas between 500 and 10,000 m², have been installed and are successfully operating for fresh-air heating in

Canada, the United States, Germany, and Japan and heating process air for crop drying in countries throughout the world.

The Hottel-Whillier (H-W) equation (Duffie and Beckman, 1991), which is customarily used to model standard flat plate solar collectors, can be made to model the UTC as well. For an unglazed collector, the H-W equation takes on the form: $\eta = F_R \alpha_s - F_R U_L (T_i - T_\infty) / G$, where η is the efficiency, α_s is the plate solar absorptivity, U_L is the heat loss coefficient, T_i is the fluid inlet temperature, T_∞ is the ambient air temperature, G is the incident solar irradiance, and F_R is the heat removal factor. For the UTC, the fluid to be heated is air taken straight from ambient, so $T_i = T_\infty$, and the equation reduces to $\eta = F_R \alpha_s$. Current theoretical modelling is aimed at determining the heat removal factor, F_R , appropriate to the UTC.

Such modelling started with the work of Kutscher *et al.* (1991), and the more recent modelling work has been summarized by Hollands (1998). Kutscher *et al.* (1991) argued that, under the range of wind and suction speeds relevant for the UTC operating with moderate temperature rises, there should be no significant

† Author to whom correspondence should be addressed.

Tel.: +1-519-888-4043; fax: +1-519-888-6197;

e-mail: kholland@solar1.uwaterloo.ca

convective heat loss from the UTC. Long-wave radiative heat transfer from the plate to the surroundings remains as the only important heat-loss mechanism (it should be noted, however, that convection is still important, in that it is the convective heat transfer between the plate and the air that is decisive in establishing the plate temperature and the radiant loss). Assuming an isothermal plate, Kutscher *et al.* (1991) developed an expression for the collector efficiency that (with an appropriate interpretation of h_r) can be made to reduce to

$$\eta = \alpha_s / (1 + h_r / (\epsilon \rho C_p V_s)) \quad (1)$$

where h_r is the radiative heat loss coefficient from plate to ambient, V_s is the superficial suction velocity (rate at which air is sucked through the plate, per unit plate area), ρ and C_p are the density and specific heat of the air, respectively, and ϵ is the 'heat exchange effectiveness', to be defined presently. This means that the H-W equation applies to the UTC provided that one takes $1/(1 + h_r/(\epsilon\rho C_p V_s))$ to be the appropriate UTC expression for F_R . In practice, values of η ranging from 50 to 80% have been commonly achieved, with V_s ranging from 0.03 to 0.08 m/s.

The key item in the above equations for η and F_R is the effectiveness, ϵ , defined by

$$\epsilon \equiv \frac{T_0 - T_\infty}{T_p - T_\infty}, \quad (2)$$

where T_0 is the mean air temperature leaving the plate at the back-side, T_∞ is the ambient air temperature, and T_p is the plate temperature. (A similar equation for ϵ can be readily derived for the case where the plate temperature varies from the isothermal state assumed by Kutscher *et al.*; in this case, T_p is to be interpreted as the mean temperature of the outside surface of the plate. A further discussion on this point is given in Appendix A.) Effectiveness, ϵ , has to be evaluated, either from experimental data, or from analysis, but, once it has been evaluated, determining η and F_R is straightforward.

The expression for ϵ will depend on how the holes are laid out on the plate, and it will also depend on the nature of the wind. Cao *et al.* (1993), Golneshan (1994), and Golneshan and Hollands (1998, 2000) reported numerical and experimental correlation equations for ϵ for a plate with holes in the form of an array of slits, the wind being assumed to be transverse to the slits but parallel to the plate. Kutscher (1994) presented an empirical model for relatively thin

plates, with circular holes on a triangular layout, with the wind parallel to the plate (grazing wind). Using computational fluid dynamics (CFD) methods, Arulanandam *et al.* (2000) analysed a plate having circular holes on a square layout, obtaining a correlation equation for the corresponding ϵ , but only under no wind conditions, and only accounting for the heat transfer on the front face of the plate and in the holes (i.e., it neglected the heat transfer at the back of the plate). Gawlik (1995) investigated the effect of having a low plate conductivity and the effect of corrugating the plate.

This paper presents new experimental data for thick and thin plates with circular holes on a square or triangular layout over a range of typical suction velocities and wind speeds, including zero wind. It extends the data of Kutscher to a wider range of plate thicknesses and hole pitch, as well as to the square pitch layout. In the region where the two studies overlap, the agreement between the two sets of data is very good, generally within about 3%, which is comparable to the accuracy of the experiments. A new predictive model is proposed for the effectiveness; one that gives a breakdown of the contribution to the heat transfer on each of the parts of the plate: that is, on the outside face, the hole, and the back of the plate. The additional information contained in this breakdown should be useful for plate-design purposes.

2. EXPERIMENTAL

Nine test plates, each 0.6 by 0.6 m and with circular holes, were constructed according to the properties listed in Table 1. The pitch P shown represents the shortest distance between adjacent holes. Plates numbered 2 to 9 had the holes on a square pitch, whereas Plate 1 had the holes laid out on a triangular pitch. (In other words, if straight lines joined the centres of adjacent circles, the lines would form a set of squares for Plates 2–9 and a set of equilateral triangles for plate 1.) The properties of plate 1 were identical to one of the plates tested by Kutscher (1994), all of whose plates had the holes laid out on a triangular pitch. Having one of the plates identical to one of Kutscher's permitted a direct comparison between the two studies. At the same time, having the rest of the plates on a square pitch permitted the square-pitch model of Arulanandam *et al.* (2000) to assist in interpreting the experimental results, as will be seen.

The effectiveness of each plate was measured

Table 1. Characteristics of the test plates

Plate no.	Plate material	Hole pitch P (mm)	Hole diameter D (mm)	Plate thickness t (mm)	Plate thermal conductivity k (W/mK)
1	Alum.*	16.89	1.60	0.86	186
2	Alum.*	16.89	1.60	0.86	186
3	PVC**	16.89	1.60	1.69	0.149
4	S. Steel***	13.33	1.60	1.57	15.12
5	PVC**	13.33	0.79	3.11	0.149
6	PVC**	8.00	1.20	6.51	0.149
7	PVC**	24.00	3.60	1.60	0.149
8	S. Steel***	24.00	3.60	0.57	15.12
9	PVC**	6.67	0.93	1.97	0.149

*Alum., aluminum; **PVC, polyvinyl chloride; ***S. Steel, stainless steel.

on the test rig developed by Golneshan (1994) and Golneshan and Hollands (1998, 2000), which is sketched in Fig. 1. Primary components of the rig included: (a) a solar simulator (or short-wave radiant heat source), (b) an air suction system for drawing air through the plate at a known rate, (c) an open-ended wind tunnel to provide a simulated wind, and (d) a data acquisition system with its associated software. A short-wave irradiance of about 700 Wm^{-2} was delivered to the entire test plate by the solar simulator, which consisted of a 49 halogen light bulb array and a 'mirror duct' lined with highly reflective metalised plastic laminate. The short-wave irradiance that was uniform to within $\pm 3\%$ over the entire test plate and within $\pm 1\%$ over the plate's 'test area', which is the inner part, excluding the part within 0.12 m of

the plate edge. The plate under test was installed on top of the suction plenum, which, itself being divided into seven equal-area compartments, divided the plate into seven corresponding sections. The four plate sections outside the test area were put there to protect against edge effects.

The experiment was designed to measure the effectiveness in the 'asymptotic region', under grazing wind conditions. Under grazing wind conditions, boundary layers, both thermal and hydrodynamic, will develop from the leading edge, and the boundary-layer thicknesses will grow with downstream distance, until eventually a steady thickness is established. This region over which the boundary-layer thicknesses is essentially invariant with the downstream distance constitutes the asymptotic region. The region between

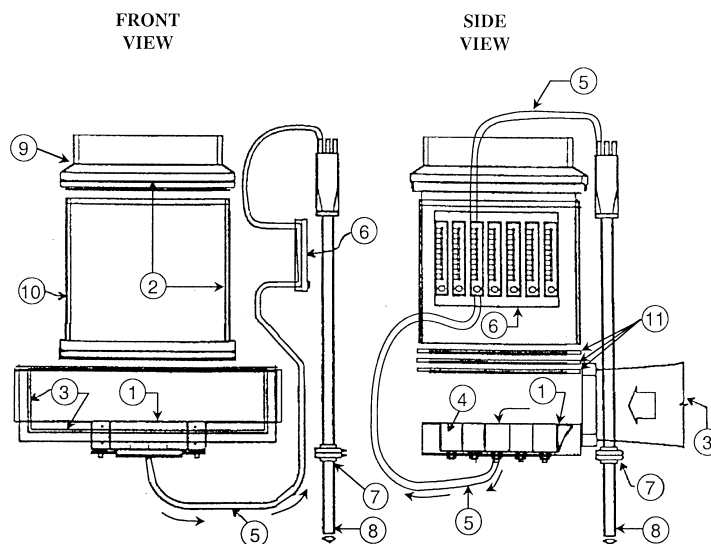


Fig. 1. Drawing of experimental apparatus. The mechanical support structure keeping the components in position has been deleted for clarity. Legend: (1) plate under test; (2) short-wave radiant source (solar simulator); (3) open circuit wind tunnel providing grazing wind to plate; (4) air plenum compartment; (5) tube carrying air flow from one plenum compartment (only one tube is shown, for clarity); (6) bank of rotameters for monitoring air flow through the different plenum compartments; (7) orifice plate for measuring total air flow; (8) pipe leading to blower sucking the air through the system; (9) set of halogen lamps [a component of (2)]; (10) a 'mirror duct' for guiding light from the halogen lamps to the plate [a component of (2)]; (11) three cooled glass sheets that shield the long-wave radiation from the lamps.

the leading edge and the asymptotic region is the starting length region. By eliminating from consideration those sections of the plenum that are in the starting length region, the measurements are ensured to be relevant to the asymptotic region¹. In practice, only about one-third or less of the plate was found to be in the starting-length region. Details of this plenum section elimination process are given by Van Decker (1996), who followed a technique developed by Golneshan (1994).

As can be seen from the defining equation for the effectiveness, [Eq. (2)], determining the effectiveness requires only the measurement of three temperatures. Fifty thermocouples were fitted at different locations on each test plate, so that the average plate temperature, T_p , could be determined. (Details of the averaging are given by Van Decker (1996).) The temperature, T_∞ , of the approaching air (i.e., the simulated wind) temperature was measured inside the wind tunnel, about 1 m upstream of the plate, with two shielded thermocouples. Additional thermocouples measured the temperatures, T_o , of the air exiting from each plenum section. The values of the effectiveness in each plenum section in the asymptotic region were averaged, and it is this average value that will be reported here.

Determining whether a given test-plate section was in the starting length required one to perform an energy balance on the subject plate section, which required knowledge of both the short-wave and long-wave radiation on the test plate. These were obtained from a solar pyranometer, and from thermocouples that measured the room temperature and the temperature of the bottom-most of the three glass plates. Located at the bottom of the reflector section, these glass plates acted as multiple long-wave radiant 'shields' between the halogen lamps and the test plate. The energy balance also required a knowledge of the short-wave absorptivity and the emissivity of the (black-painted) surface of the test-plates, both of which had been measured with reflectometers.

Each observation first required that the appropriate wind and suction flow rates be set by adjusting the wind tunnel and the suction system. After steady state was reached, measurements

were made of the wind velocity and the suction flow rate. Measurements were then taken of all the thermocouple and pyranometer *emfs*. Each plate (except Plate 2) was tested over the same set of wind and suction velocity combinations. The wind velocity range was from 0.0 m/s (no wind) to 5.0 m/s, and the suction velocity range was from 0.028 to 0.083 m/s.

With regard to experimental uncertainty in the measurements of ϵ , we first mention that Golneshan and Hollands (1998, 2000) analysed the errors in their experiments, obtaining a possible bias error of 1.5% and a random error of 0.6%. In the present work, Golneshan and Hollands' evaluation of the bias error was considered to apply in the present experiments as well, but the random error was re-estimated, by performing each experimental set-up twice and observing the deviation of the mean of the two results from the other reading. The sum of squares of these deviations over all of the experiments was converted to a 95% confidence limit of the random error in ϵ , giving 0.016. Combined with the bias error, this gave a total experimental uncertainty equal to $[(0.016)^2 + (0.015\epsilon)^2]$, a quantity that ranged from 0.017 to 0.021, depending on the value of ϵ .

The rig and experimental method had already been tested for consistency by Golneshan (1994) and Golneshan and Hollands (1998, 2000). For example, measurements had been made of the effectiveness under different intensities of the radiation from the solar-simulator. According to heat-transfer theory, the effectiveness should be independent of the magnitude of this intensity, and this had been borne through in experiments that found that, over a short-wave intensity range from 600 to 900 Wm^{-2} , the measured ϵ varied by about 0.3%, which is within the experimental error. As a check on the present work, a comparison was made with the experimental results of Kutscher. Plate 1 of the present experiments was identical to Plate 15 of the Kutscher study. However, because the experiments did not match precisely in the exact choices of wind speed and suction velocity, a direct comparison was still not possible. On the other hand, by plotting, as shown in Fig. 2, both results against the effectiveness predicted by the Kutscher model, a suitable method of comparison was afforded. According to these results, the two experiments yielded results that agreed very well, certainly within the combined experimental error of the two experiments. This added support to the integrity of the present experiments.

¹The reason for restricting measurements to the asymptotic region is that in a full-scale solar collector, say one covering the complete side of a building, the vast majority of the collector is in the asymptotic region, because starting length is generally less than about 0.25 m (Kutscher *et al.*, 1991).

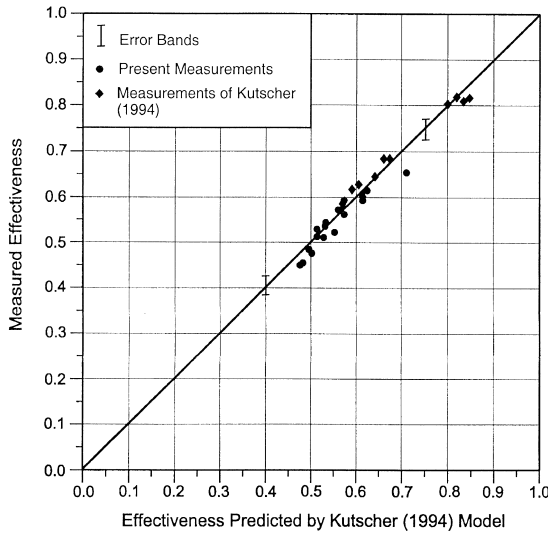


Fig. 2. Check on present experiments afforded by comparing the present results for Plate 1 to those measured by Kutscher (1994) on a plate of the same dimensions, with the same hole layout (triangular pitch) and material.

3. RESULTS

For the range of parameters studied, the effectiveness, ϵ , was found to range from a low of 0.32 to a high of 0.91. Plots were prepared (Van Decker, 1996) of ϵ against each of the relevant parameters: suction velocity, V_s , wind speed, U_w , hole pitch, P , plate thickness, t , hole diameter, D , and plate thermal conductivity, k . Effectiveness, ϵ , was found to decrease with increasing V_s , P , and D , and to increase with increasing U_w and with t . The strongest effects were found to be attributable to V_s and P , while the effectiveness was found to be only very weakly dependent on plate thermal conductivity, k . All of these observations are consistent with the findings of Kutscher (1994), except for the effects of k and t , which were not studied by Kutscher. The effect of t was not unexpected, as a thicker plate has the increased heat-transfer area associated with the sides of the holes.

The degree to which the plates were isothermal was also tested. It was found that the maximum variation in plate temperature was for Plate 7, which had the lowest plate conductivity and the largest pitch of all the plates. In this case, the variation was $\pm 2.5^\circ\text{C}$ from the average plate temperature. For the other PVC plates, the variation was much less, and for the metallic plates, it was essentially zero.

The work of Golneshan and Hollands (1998, 2000) had suggested that the combined dimen-

sionless variable γ , defined by $\gamma = V_s^2 P / U_w k$, should characterize the heat transfer at the front surface of the plate, at least under conditions of significant wind. Since most of the heat transfer was expected to occur at the front surface of the plate, and since γ contains all three of the most important variables, this combined parameter would seem to be a good choice to plot effectiveness against, in order to get a general perspective on the nature of the data. Fig. 3 shows such a plot of all the 'windy' data (i.e., all the data excluding those with zero wind). It is clear from the plot that although a dependence on γ accounts for much of the spread of the data, there are other dependencies, which, if the suggestion of Golneshan and Hollands is correct, must all be attributable to the heat transfer in the holes and at the back of the plate.

Plates 1 and 2 have the same values of t , D , k , and P (P being the shortest distance between two holes). However, the holes on Plate 1 had been laid out on a triangular pitch and the holes on Plate 2 on a square pitch. Over the experimental range covered, Plate 1 was found to have an average ϵ that was 0.05 higher than the ϵ for Plate 2. That is, other things being equal, the triangular layout performs slightly better. Both plates had the same values of t and k as the Kutscher plates, so Kutscher's model would be expected to apply for Plate 1. This being the case, the value of P to be used in Kutscher's model for the square-pitched plate was adjusted by a constant factor until the average deviation between the predicted ϵ from the Kutscher model and the measure ϵ was minimized. The constant factor (called the pitch scaling factor) was found to be 1.6. This means that the Kutscher model (derived for a triangular layout) can presumably be modified so as to apply to plates with the holes on a square layout, if the pitch used in the Kutscher model is taken as 1.6 times the minimum distance between the holes on the square layout.

This modified Kutscher model could now be used to predict the present results for Plates 2–9. The comparison between the predicted and measured results is shown in Fig. 4. The root mean square difference between the measured values of ϵ and the values predicted by the model was about 0.06, or an average of about 10.6% of the average measured value of ϵ . However, the model under-predicts the results for Plate 6, by a large amount, i.e., about 20%. Plate 6, it should be noted, is the plate with the largest value of t , and since none of Kutscher's plates had such a large value of t and the effect of t was not studied by

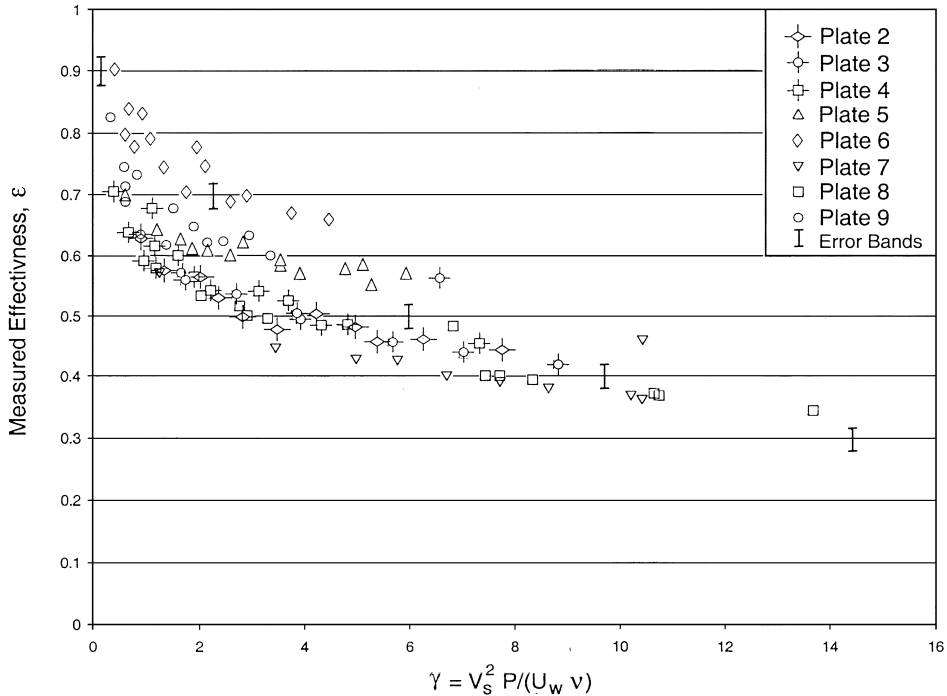


Fig. 3. Presentation of the 'windy' experimental results, in the form of a plot of the effectiveness versus the dimensionless group γ . Results on all the plates except Plate 1 are shown.

Kutscher, such a large difference was not unexpected. (As will be explained later, there is significant heat transfer in the hole, and since this heat transfer is proportional to the area of the hole, the hole heat transfer will be greater for thicker plates.) Generally, and under typical oper-

ating conditions, a 10% (20%) error in predicting ϵ will produce a 5% (10%) error in predicting the efficiency, and so, it would appear to be useful to seek a new model that predicts results more accurately than the Kutscher model, which was the goal of the work described in the following section.

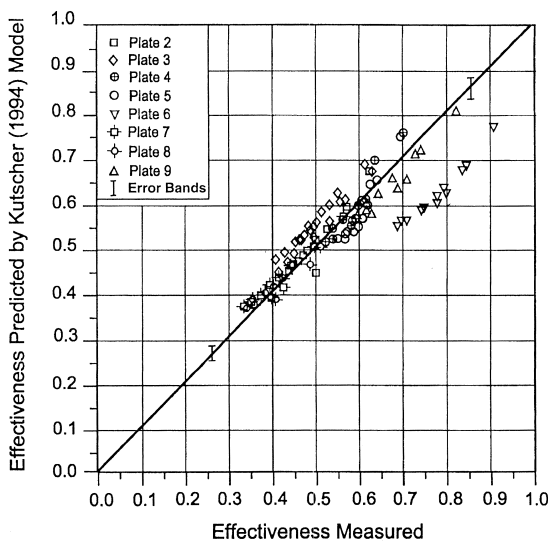


Fig. 4. Comparison of the measured effectiveness with the corresponding effectiveness predicted using the model of Kutscher (1994) revised to incorporate the square pitch layout by altering the pitch.

4. MODEL DEVELOPMENT

The model development presented in this paper assumes that the plate is isothermal. In reality, mainly because the local convective heat transfer coefficient is much greater in and near the holes than elsewhere, there will be some non-isothermality, the magnitude of which will depend upon the plate conductivity k (see Appendix A). Each aluminum plate was found to behave, for practical purposes, like an isothermal plate, but with the PVC plates, some modest degree of temperature non-uniformity was observed, as was already reported. Because the effect of k on ϵ was found to be weak, an isothermal model will be used in this paper.

For the purposes of analysis, the total air-heating effect of the plate can be separated into that in three regions on the plate surface: the front-of-the-plate, the hole, and the back-of-the-plate. Each region can be assigned an effective-

ness (making three effectivenesses in all, denoted as ϵ_f , ϵ_h , and ϵ_b , respectively):

$$\epsilon_f \equiv \frac{T_{o1} - T_\infty}{T_p - T_\infty}, \quad \epsilon_h \equiv \frac{T_{o2} - T_{o1}}{T_p - T_{o1}},$$

$$\epsilon_b \equiv \frac{T_o - T_{o2}}{T_p - T_{o2}} \quad (3)$$

where T_{o1} is the bulk mean temperature of the air as it enters the hole and T_{o2} is the bulk mean temperature of the air as it exits the hole (see Fig. 5). We can also define a combined effectiveness, ϵ_{fh} , for the front of the plate plus the hole as

$$\epsilon_{fh} \equiv \frac{T_{o2} - T_\infty}{T_p - T_\infty}. \quad (4)$$

From Eqs. (2)–(4), it is easy to show that

$$\epsilon = 1 - (1 - \epsilon_f)(1 - \epsilon_h)(1 - \epsilon_b) \quad (5)$$

and

$$\epsilon = 1 - (1 - \epsilon_b)/(1 - \epsilon_{fh}). \quad (6)$$

As the mechanisms for convective heat transfer tend to be different in each plate part, the model development will consider each part separately, starting with the heat transfer at the back of the plate.

4.1. Back-of-plate heat transfer

As the flow emerges from the hole as a jet at the back-side of the plate, it will tend to break into relatively large recirculating turbulent eddies that will wash the back surface of the plate, cooling the plate. Since the jet has broken away (or separated) from the wall, this type of flow constitutes separated flow. Heat transfer in separated flow has been treated in the heat transfer

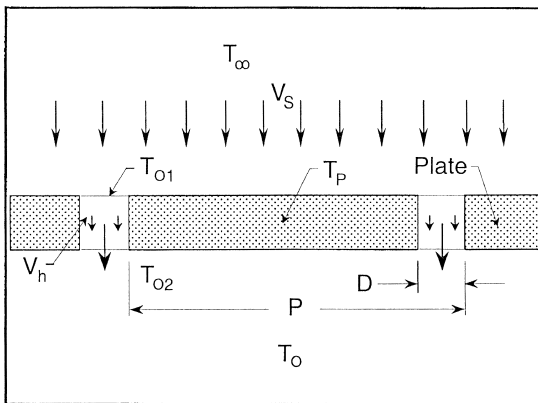


Fig. 5. Sketch to define the temperatures T_{o1} and T_{o2} , which are the bulk air temperatures entering and leaving the hole, respectively.

literature (for example, see Zukaurkas and Zingzda, 1985), although none of the available heat-transfer correlations in the literature relate to the present geometry. One way to assess the magnitude of this back-of-the-plate heat transfer using the present data was to compare the measured effectiveness under no-wind conditions to the effectiveness predicted by the CFD-derived model of Arulanandam *et al.* (2000). The latter predictions were predictions only of ϵ_{fh} , i.e., they account for the effect of the heat transfer on the front of the plate and in the hole, but they do not account for the back-of-the-plate heat transfer, which, associated with separated flow, tends to be rather difficult to predict using CFD methods. Arulanandam *et al.* (2000) gave a correlation equation for ϵ_{fh} that covered the full range of the zero-wind runs of the current experiments. Fig. 6 plots the ϵ_{fh} calculated from their correlation equation against the measured no-wind ϵ . The predictions are consistently below the measured results, as one would expect, since the predictions do not account for the heat transfer at the back of the plate.

After inserting into Eq. (6) each measured value for ϵ and each corresponding value for ϵ_{fh} predicted by the Arulanandam *et al.* model, the back-of-the-plate effectiveness, ϵ_b , was calculated for each data point in Fig. 6. On finding the resulting values of ϵ_b to be not totally constant (even after allowing for experimental error), an equation was derived that would model the depen-

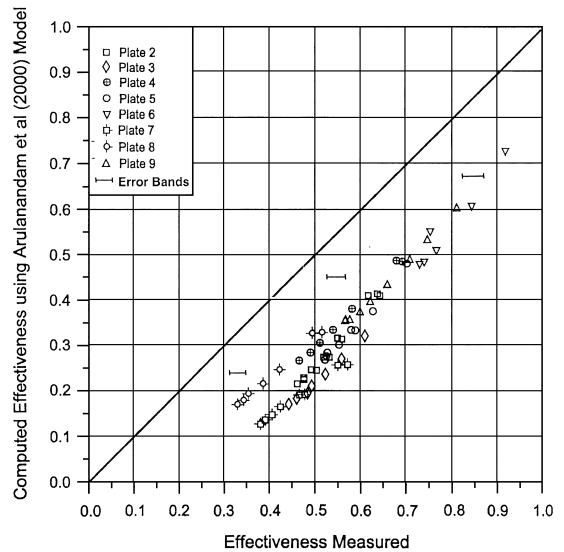


Fig. 6. Comparison of Arulanandam *et al.*'s model with the present measurements. The CFD-based Arulanandam *et al.* model does not account for the heat transfer at the back of the plate.

dence of ϵ_b on the dimensionless groups that it was thought to depend on, using existing models for heat transfer in separated flow as a guide. Assuming the air in the region behind the plate was well mixed by the turbulent eddies, it is easy to show that $\epsilon_b = (1 + St_b^{-1})^{-1}$ where St_b is the Stanton number at the back of the plate, given by $St_b \equiv h_b / (\rho V_s C_p)$, in which h_b is the convective heat-transfer coefficient at the back of the plate. Examination of the separated flow literature suggested that St_b can be expected to correlate with the relevant Reynolds number with a power law relation, with a power coefficient of about $-1/3$. It was found that it could be well correlated against a particular Reynolds number, denoted Re_b , which is equal to $V_h P / \nu$, in which $V_h = V_s / \sigma$ is the velocity in the hole, with σ being the plate porosity, which is equal to $\pi D^2 / 4P^2$ for holes on a square pitch. The correlation equation was $St_b = 6.93 Re_b^{1/3}$. Thus, the model for ϵ_b took the form

$$\epsilon_b = \frac{1}{1 + e Re_b^{1/3}}, \quad (7)$$

with $e = 0.144$. (This was a tentative, preliminary values for e ; like other free parameters to be introduced later, they were slightly revised later, based on a 'global fit' to the data.)

It will be recalled that the above development was based on a CFD model and data that are restricted to zero-wind conditions. When one considers whether this same model can be safely used for 'windy' conditions, one must consider whether the flow at the back of the plate will be significantly altered by the presence of the wind. Certainly, the jet of air emerging from the hole will contain some finite component of the down-wind momentum, carried, through conservation of momentum, from the free-stream region on the other side of the boundary layer. However, this momentum can be expected to be relatively small, for two reasons. First, before it reaches the hole, the down-wind component of the air is, in passing through the boundary layer, decreased considerably (if not reduced to zero) by the demands of the non-slip boundary condition on the plate surrounding the hole, and it is further decreased in the hole. Second, the wind speed was smaller than, or at most of the same order as, the actual velocity in the hole; typically the velocity in the hole was of the order of 5 m/s, while the wind speed was of the order of 2 m/s. For these reasons, and in view of a dearth of other information, the back-of-the-plate heat transfer will be assumed to be independent of the presence of

the wind. This means that Eq. (7) can be applied to the other data points, not just the zero-wind cases.

By combining Eqs. (6) and (7), the combined front-of-plate and hole effectiveness, ϵ_{th} , could then be estimated for each data point, using

$$\epsilon_{th} = 1 - \frac{1 - \epsilon}{1 - (1 + 0.144 Re_b^{1/3})^{-1}}. \quad (8)$$

4.2. Front-of-plate heat transfer

Two dimensionless groups, both Reynolds numbers, would seem to be important in establishing the heat transfer on the front face of the plates: one, Re_w , based on the wind speed and the other, Re_s , based on the suction velocity; thus one has $Re_w = U_w P / \nu$ and $Re_s = V_s P / \nu$. For the zero-wind condition, Re_s should be the only important Reynolds number.

Golneshan (1994) developed a momentum integral analysis for the UTC in 2D flow (i.e. with slit-like instead of circular holes) for windy conditions. Heat transfer on the front of the plate was found to be dependent upon a single parameter, γ , a combination of Re_w and Re_s defined by:

$$\gamma = Re_s^2 / Re_w = V_s^2 P / U_w \nu. \quad (9)$$

The experimental study of Golneshan and Hollands (1998, 2000) in plates with slit-like perforations under windy conditions showed that, indeed, this single group captured the combined effect of suction velocity and wind speed. Moreover, they found that the data fit the form of the dependence of ϵ_f on γ that had been predicted by the integral analysis, namely²

$$\epsilon_f = (1 + a \gamma^{1/2})^{-1} = (1 + a Re_s / Re_w^{1/2})^{-1} \quad (10)$$

where a is a constant parameter. Although Eq. (10) was derived for 2D flow, it seemed appropriate to

²Actually, Golneshan and Hollands derived the equation: $\epsilon_f = 1 - (b + a^{-1} \gamma^{-1/2})^{-1}$, which contains an additional parameter, b , but which reduces to Eq. (10) when $b = 1$. However, for suitable values for b , the Golneshan and Hollands equation yields negative values for ϵ_f when γ is very large, as γ will be in a very low-wind situation. Consequently, their equation was simplified to Eq. (10), for the present work where it was important to accommodate low wind situations. This simplification was not found to introduce an appreciable penalty in fitting the data at high wind speeds. It should be noted that, even though it incorporates this revision, Eq. (10) is unsuitable for zero-wind conditions; when $U_w = 0$, γ goes to infinity, and ϵ_f would go to zero, a result that is not observed in practice. A correction for this fact is described later.

see if its form was suitable for the present problem of flow approaching circular holes, and such a check is now described.

If it were not for the heat transfer in the holes, one would have $\epsilon_f \approx \epsilon_{th}$. Plates 7 and 8 were expected to have very small heat transfer at the hole because they were so thin and their hole diameters were relatively large (as the next section will show, ϵ_{th} tends to decrease with increasing D as well as decreasing t). Thus, it was assumed that $\epsilon_f \approx \epsilon_{th}$ for Plates 7 and 8, and using this equality in addition to Eq. (8), ϵ_f was calculated for each windy data point measured on these plates. Satisfying Eq. (10) demands that a plot $1/\epsilon_f - 1$ vs. $\gamma^{1/2}$ should yield a straight line passing through the origin, the subject data were plotted in this manner. Fig. 7 shows the results, also showing the error bounds on the quantity $(1/\epsilon_f - 1)$. [These error bounds are quite large; although the uncertainty in ϵ was only about 0.019, this uncertainty was transformed into much larger values after the transformation from ϵ to $(1/\epsilon_f - 1)$.] Two things are to be observed in this plot. First, despite the different geometric characteristics of Plates 7 and 8, their data run close to a common curve. Second, the common curve is close to a straight line passing through the origin, as the theory would predict. While the best linear fit to the data (the solid line shown) would not pass within the (95% confidence) error bounds of all the points, it would fall within the range of all but a few. Moreover, there exists one straight line that does pass within the error bounds of all of the

curves. So, overall, the fit of the model to the data was remarkably good, so it was decided to adopt Eq. (10) for the model for all the (windy) data, choosing the value of parameter a on the basis of a global fit. A preliminary estimate, based on Plates 7 and 8, gave $a \approx 1.72$.

Eq. (10) is not suitable for the zero-wind situation because, at $Re_w = 0$, it predicts that $\epsilon_f = 0$, a result that is not observed in practice. On the other hand, the zero-wind situation was covered by the Arulanandam *et al.* model, so one could use this model at zero-wind. Nevertheless, it would be preferable for practical calculations to have a single model that goes continuously from the zero-wind situation to the windy situation. Such a practical model would perhaps not be as accurate at zero wind as the Arulanandam *et al.* model, but a situation of exactly no wind is uncommon in practice, so high accuracy is not needed for that situation; moreover, it would appear that the model of Eq. (11) is reasonably accurate for the smallest wind speeds for which measurements were made, namely, a wind speed of 0.8 m/s, so the wind-speed range not necessarily covered by either model was the relatively narrow one: $0 > U_w > 0.8$ ms, which is rarely encountered in practice, as average wind speeds are typically of the order of 5 m/s. After examining both the Arulanandam and Hollands models and the zero-wind data for Plates 8 and 9, the zero-wind situation was found to be adequately covered by a model quite similar to Eq. (10), namely

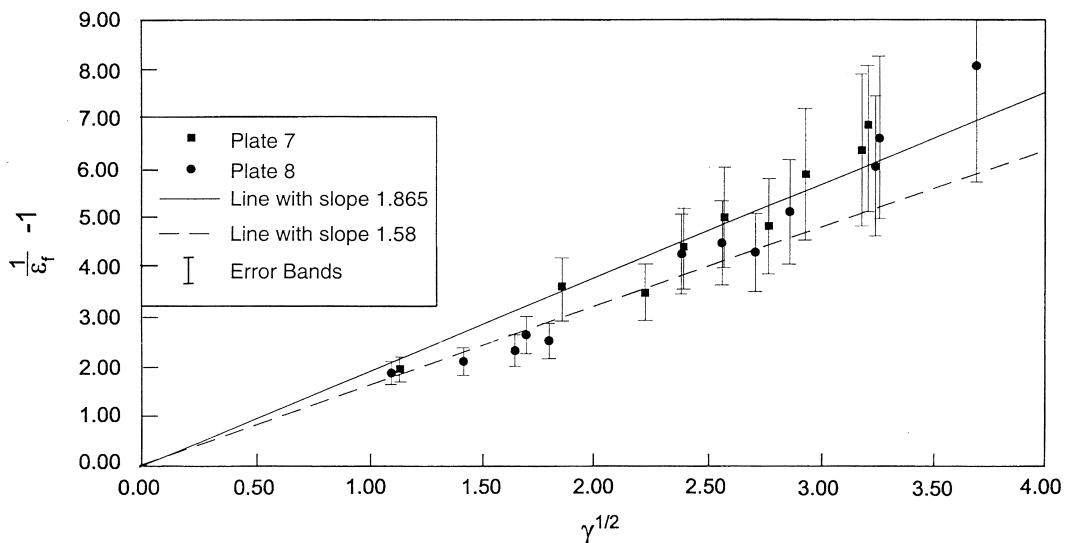


Fig. 7. Test of Eq. (10) (Golneshan, 1994) for modelling the front of the plate effectiveness. The data should plot as a straight line. The solid straight line is a least-squares linear fit to the data, and the dashed line lies within experimental error of all of the points.

$$\epsilon_f = \frac{1}{1 + fRe_s} \quad (11)$$

where f is constant, equal to 0.0654.

Eq. (11) applies in the zero-wind situation and Eq. (10) in the windy situation. It is proposed that they be combined into the single equation

$$\epsilon_f = \frac{1}{1 + Re_s \min[aRe_w^{-1/2}, f]} \quad (12)$$

where the symbol ‘ $\min[x, y]$ ’ means that one is to take the minimum of x and y . Because of the nature of the $\min[x, y]$ function, one finds that the equation automatically shifts to Eq. (11) for zero-wind conditions ($Re_w = 0$), and Eq. (10) is found to apply whenever Re_w is greater than $(a/f)^2$, which was found to be about 700, and, since almost all of the ‘windy’ data points have Re_w greater than 700, the model will reduce to Eq. (10) for the windy experimental conditions.

4.3. Heat transfer in the hole

The model for ϵ_h can safely assume laminar flow in the hole, since the hole Reynolds number, $Re_h = V_s D / (\nu \sigma)$, was found to be much less than 2000. Provisionally, one can treat the flow in the hole as (hydrodynamically and thermally) developing flow inside an isothermal circular cylinder, for which there is ample information in the literature (Incropera and DeWitt, 1990). Hole effectiveness is then given by:

$$\epsilon_h = 1 - \exp^{-NTU}, \quad (13)$$

in which

$$NTU = \frac{h_h \pi D t}{m C_p} \quad (14)$$

where h_h is the average heat transfer coefficient in the hole, and $m = \rho P^2 V_s$ the mass flow rate of air through the hole. The heat-transfer coefficient h_h is to be calculated from the average Nusselt number, Nu_h , in the hole: $h_h = Nu_h k_{air} / D$. Treating the hole as a cylinder with a length equal to the plate thickness, t , and tube diameter, D , the hole Nusselt number is a function of the Graetz number, $Gr_h = Re_h Pr D / t$ (Ebdian and Dong, 1998). The function can be approximated as linear: that is, by

$$Nu_h = 3.66 + \bar{c} Gr_h \quad (15)$$

with \bar{c} approximately equal to 0.1. This model satisfies the well-established requirement that $Nu_h = 3.66$ when Gr_h is very small, i.e., when the flow in the cylinder is fully developed.

With a model for ϵ_f and ϵ_b at hand from previous sections, one can calculate ϵ_h for every data point, and use this data set for testing or calibrating a model for ϵ_h . On this basis, the model constituted by Eqs. (13)–(15) was tested, and the results fit the data reasonably well, but not as well as would have been expected. The reason was that Eq. (15) was based on the assumption that the fluid enters the cylinder at a uniform temperature, whereas the air entering the hole will be non-uniform; the air nearer the plate will be hotter than that near the centre-line. The non-uniformity of the air-temperature distribution will be greater with increasing P and decreasing D . To capture this effect, parameter \bar{c} was made a function of P/D . A proportional dependence was found to give an excellent fit to the data, so \bar{c} was made equal to cP/D , where c , a parameter to be chosen on the basis of a fit to the data, was found to be given by $c = 0.0047$. Combining the above equation gives

$$\epsilon_h = 1 - \exp \left[-4 \left(c \frac{P}{D} + \frac{3.66}{Pr Re_h} \frac{t}{D} \right) \right] \quad (16)$$

which is the model for the hole effectiveness.

4.4. Global regression fit and overall model

Eqs. (5), (7), (12) and (16), with appropriate values for the parameters, constitute a predictive model for the overall effectiveness, ϵ . The constants have been assigned preliminary values based on the partial fits discussed in previous sections. However, to eliminate any bias associated with these limited data sets and to minimize the overall effects of any tenuous assumptions (such as assuming wind does not effect the heat transfer at the back of the plate or assuming that there was no significant hole heat transfer for Plates 7 and 8), a global fitting process was entered into whereby the sum of the squares of the deviations between model and measurement over the full set of data points was minimized. The results of this gave $e = 0.2273$, $a = 1.733$, $f = 0.02136$, and $c = 0.004738$. In summary (after making $Pr = 0.71$ for air and making several other substitutions), the total effectiveness model for a UTC with a square-hole geometry is given by:

$$\begin{aligned} \epsilon = & \left[1 - (1 + Re_s \max[1.733 Re_w^{-1/2}, 0.02136])^{-1} \right] \\ & \times \left[1 - (1 + 0.2273 Re_b^{1/2})^{-1} \right] \\ & \times \exp \left(-0.01895 \frac{P}{D} - \frac{20.62}{Re_h} \frac{t}{D} \right) \end{aligned} \quad (17)$$

This model was found to fit all of the data (both windy and zero-wind) for plates with holes laid

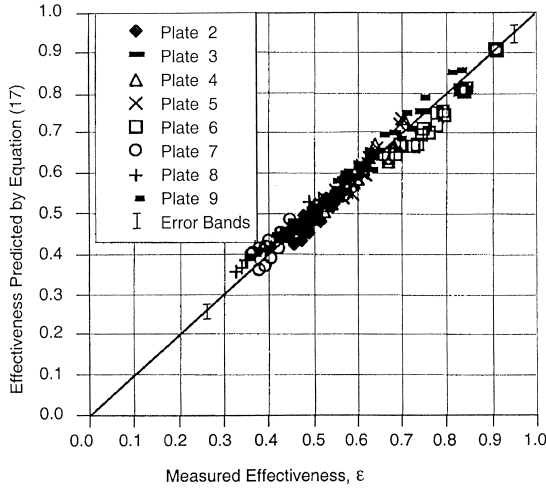


Fig. 8. Comparison of Eq. (17) with the results measured on plates with holes on a square pitch.

out on a square pitch, with a root mean square error of 4.3%. Fig. 8 compares the data to the model, by plotting the model prediction on one axis and the measured result on the other.

4.5. Testing the model on a triangular-pitched plate

It was shown previously that a triangular-plate model (like that developed by Kutscher) can be used for a square pitched plate if one uses for the pitch, P , a value that is ξ times the square layout pitch, where 'scaling factor', ξ , is equal to 1.6. Conversely, a square-plate model [like Eq. (17)] can be used for a triangular pitched plate, if one uses for the pitch, P , a value that is $1/\xi$ times the triangular layout pitch, where, again, scaling factor ξ is equal to 1.6. This means that Eq. (17), with this proviso, predicts results for triangular plates, so it was tested on Kutscher's data, yielding the comparisons shown in Fig. 9. Excellent agreement was found. The root mean square relative deviations between the predictions and the measured data were found to be 6.6%. Also, the mean bias error in the model was found to be essentially zero. Thus, Eq. (17) predicts Kutscher's data with almost the same fidelity as it fits the present data. That the fidelity is not so great may be attributable to a possible dependence of the scaling factor on pitch.

4.6. Relative contributions of regions

A useful feature of the model is that it provides information on the contribution to the overall heat transfer provided by each of the three regions: the front-of-plate, the hole, and the back-of-plate. The important contribution of the back-of-plate and

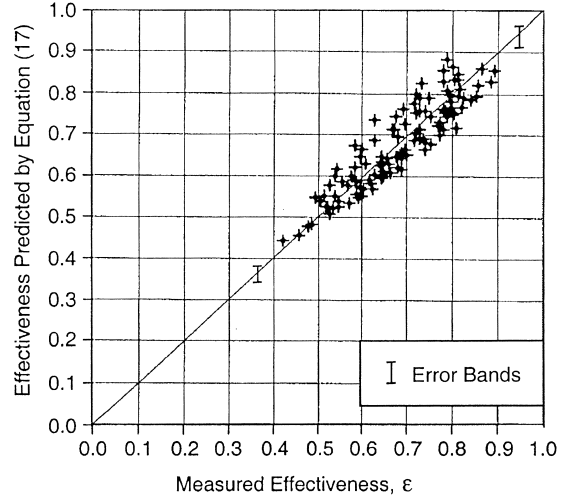


Fig. 9. A test to see how well Eq. 17 predicts the measurements of Kutscher (1994). For this comparison, Eq. (17) was revised to make it applicable to plates with a triangular pitch.

the holes is to be particularly noted. As an example, consider the following settings, which are representative of a commercial solar collector plate operating under average suction and wind-speed conditions: $P=16.9$ mm, $D=1.60$ mm, $t=0.8$ mm, $V_s=0.04$ m/s, and $U_\infty=2.4$ m/s. Under these conditions, the model predicts $\varepsilon_f=0.405$, $\varepsilon_h=0.306$, $\varepsilon_b=0.149$, $\varepsilon_{th}=0.588$, and $\varepsilon=0.649$. This means that 62% of the ultimate temperature rise of the air occurs on the front surface, 28% occurs in the hole, and 10% occurs on the back. This information constitutes useful knowledge for those trying to optimize the plate design or to develop improved plates.

5. CONCLUSIONS

Eq. (17) provides a suitable model for the thermal effectiveness, ε , for UTCs, including the case of no-wind. With suitable interpretation of the measure of pitch, it is useful for plates laid out with square and triangular hole placements. It captures the effect of a range of variables, such as, suction velocity, V_s , wind velocity, U_∞ , hole pitch, P , hole diameter, D , and plate thickness, t , having been tested over the following ranges of these variables: $0.028 \text{ m/s} \leq V_s \leq 0.083 \text{ m/s}$; $0 \text{ m/s} \leq U_\infty \leq 5.0 \text{ m/s}$; $7 \text{ mm} \leq P \leq 24 \text{ mm}$; $0.8 \text{ mm} \leq D \leq 3.6 \text{ mm}$; $0.6 \text{ mm} \leq t \leq 6.5 \text{ mm}$, as well as on plates having thermal conductivity, k , ranging from 0.15 to 200 W/mK. Under typical operating conditions, about 62% of the ultimate temperature rise of the air is predicted to occur on the front surface, 28% in the hole, and 10% on the back of the plate.

NOMENCLATURE

a	constant in Eq. (10), chosen so as to give the best fit to experimental data
A_d	dimensionless group, known as the plate admittance, $A_d = k_s t / kD$
A_{rep}	the surface area of a representative element of the plate
\bar{c}	constant in Eq. (16), equal to 0.0047
\bar{c}	constant in Eq. (15)
C_p	specific heat of air, J/kgK
D	diameter of hole, m
e	constant in Eq. (7), chosen to give the best fit to experimental data
f	constant in Eq. (11), chosen to give best fit to experimental data
F_R	solar collector heat removal factor
G	solar irradiance incident on collector, W/m ²
Gr_h	Graetz number in the hole, equal to $Re_h PrD/t$
h_r	radiative heat-transfer coefficient from plate to ambient surrounds (see Eq. (A.1), W/m ² K
h_b	convective heat-transfer coefficient between the back of the plate and the air in the plenum, W/m ² K
h_h	convective heat-transfer coefficient between a hole and the air in the hole, W/m ² K
k, k_{air}	thermal conductivity of plate material and air, respectively, W/mK
Nu	Nusselt number in the hole, equal to $h_h D / k_{air}$
Nu_r	radiation Nusselt number, $Nu_r = h_r D / k$
NTU	number of transfer units for hole heat transfer, defined by Eq. (14)
P	pitch of the holes on the plate, equal to the shortest distance between adjacent holes, m
Pr	Prandtl number of air
Re_b, Re_s, Re_w	Reynolds numbers defined by $Re_b = V_h P / \nu$, $Re_s = V_s P / \nu$, and $Re_w = U_w P / \nu$, respectively
St	Stanton number governing heat transfer on the back of a plate, equal to $h_b / (\rho C_p V_s)$
t	plate thickness, m
T_i	inlet temperature to solar collector, K
T_o	bulk mean temperature of air leaving the back of the plate, K
T_{o1}	temperature of air as it enters a hole, K
T_{o2}	temperature of air as it leaves a hole, K
T_p	mean plate temperature, as defined by Eq. (A.2), K
$T'_p(x, y)$	local temperature at point (x, y) on the outside surface of the plate, K
$T'_{p,min}, T'_{p,max}$	the minimum and maximum values for $T'_p(x, y)$, respectively
T_∞	ambient air temperature, K
U_L	collector overall heat loss coefficient, W/m ² K
U_w	wind speed, m/s
V_h	air velocity in the hole, $= V_s / \sigma$, m/s
V_s	suction velocity (rate at which air is sucked through a plate, per unit plate area), m/s
(x, y)	co-ordinates of a point on the outside surface of the plate
<i>Greek letters</i>	
α_s	solar absorptivity of the plate
γ	dimensionless parameter defined by Eq. (9)
$\epsilon, \epsilon_r, \text{etc.}$	ϵ = plate heat exchanger effectiveness defined by Eq. (2); ϵ_r, ϵ_b and ϵ_s are defined by Eq. (3), and ϵ_{in} by Eq. (4)

η	collector efficiency
ν	kinematic viscosity of air, m ² /s
ρ	density of air, kg/m ³
σ	porosity of plate; i.e., fraction of plate's superficial area that is taken up by the holes

Short forms and special symbols

UTC	unglazed transpired-plate collector
min[x, y]	a quantity equal to x or y , whichever is smaller

Acknowledgements—The authors would like to thank the Natural Sciences and Engineering Research Council Canada for providing the financial support for this work through a research grant to the University of Waterloo. We would also like to thank Dr. Ali Golneshan for all his excellent and painstaking work in designing, setting up, and breaking in the apparatus. Thanks also to Professor Ewart Brundrett for giving us access to the wind tunnel. The experiments were performed at the University of Waterloo.

APPENDIX A. INTERPRETATION OF EFFECTIVENESS FOR NON-ISOTHERMAL PLATES

Some question may arise about the meaning of the plate's heat exchange effectiveness when the plate is non-isothermal. Considerable simplification of this issue is achieved if one is willing to adopt the familiar approximation that the relevant 'radiant heat transfer coefficient, h_r ' is essentially constant over the temperature ranges of interest. In this case, this would require assuming

$$h_r = \epsilon_p \frac{\sigma((T'_p(x, y))^4 - T_\infty^4)}{T'_p(x, y) - T_\infty} \quad (\text{A.1})$$

(where $T'_p(x, y)$ is the local outside surface temperature of the plate, and x and y are local co-ordinates on the surface of the plate) to be essentially constant, over the surface temperature range: $T'_{p,min} < T'_p(x, y) < T'_{p,max}$, where $T'_{p,min}$ and $T'_{p,max}$ are the minimum and maximum values for $T'_p(x, y)$, respectively. It is common in low-temperature solar heat transfer analysis to treat radiant heat transfer coefficients as constant over temperature ranges of 10 to 30 K or more, so it is not unrealistic to treat the h_r in Eq. A.1 as being constant over the modest range of a few degrees K that is typically experienced on the plate of a UTC.

With this approximation in hand, it is easy to show that the radiant loss, q_r , from the plate, per unit area, is

$$q_r = h_r(T_p - T_\infty) \text{ where}$$

$$T_p = \iint_{A_{rep}} T'_p(x, y) dA \quad (\text{A.2})$$

where A_{rep} is the surface area of a representative element of the plate (Arulanandam *et al.*, 2000). A heat balance on the plate leads directly to Eq. (1), so Eq. (A.2) defines the relevant mean temperature to be used in Eq. (2) when the plate is not isothermal.

As was made clear in the analysis of Arulanandam *et al.* (2000), in principle, the effectiveness, ϵ , will depend on h_r , or, in dimensionless terms, on the 'radiation Nusselt number' $Nu_r = h_r D/k$. On the other hand, their computational study, in which $Nu_r = h_r D/k$ varied from 0.13 to 0.52, showed no detectable effect of Nu_r . The present experiments covered a Nu_r range from about 0.2 to 0.9, which also corresponds to the Nu_r range covered in UTC's used in the field.

Arulanandam (1995) and Arulanandam *et al.* (2000) carried out a detailed dimensional analysis of this problem, and, although it was for the no-wind case, its extension to the case with wind is straightforward. They used the well-recognized method of first writing down the full set of governing equations and the boundary conditions, then forming dimensionless counterparts of each quantity in these equations, substituting these defining equations into the governing equations and boundary conditions, and, finally, noting the dimensionless groups that arise. Any dimensionless output quantity, such as effectiveness, must then only be a function of the dimensionless groups that arise. In addition to the relevant Reynolds numbers, t/D and P/D , this list also includes two more groups: the plate admittance, $A_d = k_s t/kD$, and the radiative Nusselt number, Nu_r . One can show that there can only be a dependence on Nu_r if there is also a dependence on A_d .

Using the new experimental data reported in this paper (which covered a range in A_d from 0.4 to 378), a study was carried out to see if there was a statistically significant effect of A_d on ϵ (Van Decker, 1996). Only a very weak dependence was found; it was found that including A_d as an additional parameter in Eq. (17) reduced the standard deviation between the model and the data by only 1%. It was concluded that the effect of Nu_r must be even less important, confirming the null findings of Arulanandam *et al.* (2000), mentioned above.

REFERENCES

- Arulanandam S. J. (1995) *A numerical investigation of unglazed transpired-plate solar collectors under zero-wind conditions*, M.A.Sc. Thesis, University of Waterloo, Waterloo, Canada.
- Arulanandam S. J., Hollands K. G. T. and Brundrett E. (2000) A CFD heat transfer analysis of the transpired solar collector under no-wind conditions. *Solar Energy* **67**(1–3), 93–100.
- Carpenter S. C. and Kokko J. P. (1991) Performance of solar preheated ventilation air systems, *Proceedings Annual Conference of Solar Energy Society of Canada Inc.*, Toronto, Canada, Solar Energy Society of Canada Inc., Ottawa, pp. 261–265.
- Cao S., Hollands K. G. T. and Brundrett E. (1993) Heat exchange effectiveness of unglazed transpired-plate solar collector in 2D flow. *Proceedings of ISES Solar World Congress 1993*, Budapest, Hungary, 5, pp. 351–366.
- Duffie J. A. and Beckman W. A. (1991) *Solar Engineering of Thermal Processes*, 2nd edn, pp. 278–279. John Wiley & Sons Inc., New York.
- Dymond C. and Kutscher C. (1997) Development of a flow distribution and design model for transpired solar collectors. *Solar Energy* **60**, 291–300.
- Ebadian M. A. and Dong Z. F. (1998) Forced convection, internal flow in ducts. In 3rd Edition, *Handbook of Heat Transfer*, Rohsenow W. M., Hartnett J. P. and Young Y. I. (Eds.), pp. 5.14–5.16, McGraw-Hill, New York.
- Gawlik K. M., (1995) *A Numerical and Experimental Investigation of Heat Transfer Issues in the Practical Utilization of Unglazed, Transpired Solar Air Heaters*, Ph.D. Thesis, Department of Civil, Environmental and Architectural Engineering, University of Colorado, Boulder, Colorado, USA.
- Golneshan A. A. (1994) *Forced Convection Heat Transfer from Low Porosity Slotted Transpired Plates*, Ph.D. Thesis, Department of Mechanical Engineering, University of Waterloo, Waterloo, Canada.
- Golneshan A. A. and Hollands K. G. T. (1998) Experiments on forced convection heat transfer from slotted transpired plates, *Proceedings CSME Forum 1998*, Toronto Canada, Canadian Society for Mechanical Engineering, Hamilton, Canada, Vol. 1, pp. 78–88.
- Golneshan A. A. and Hollands K. G. T. (2000) Forced convection experiments on slotted transpired plates. *Transactions of the Canadian Society for Mechanical Engineering* **24**(1B), 335–347.
- Gunnnewiek L. H., Hollands K. G. T. and Brundrett E. (1997) Flow distribution in unglazed transpired plate solar air heaters of large area. *Solar Energy* **58**, 227–237.
- Hollands K. G. T. (1998) Principles of the transpired-plate air heating collector: the solarwall, *Renewable Energy Technologies in Cold Climates '98 (Incorporating the 1998 Annual Conference of the Solar Energy Society of Canada, Inc.)*, The Solar Energy Society of Canada Inc., Ottawa, pp. 139–144.
- Hollick J. C. and Peter R. W. (1990) United States Patent No. 4,934,338.
- Incropera F. P. and DeWitt D. P. (1990) In *Fundamentals of Heat and Mass Transfer*, 3rd edn, pp. 494–495, Wiley, New York.
- Kutscher C. F. (1994) Heat exchanger effectiveness and pressure drop for air flow through perforated plates with and without crosswind. *J. Heat Transfer* **116**, 391–399.
- Kutscher C. F., Christensen C., and Barker, G. (1991) Unglazed transpired solar collectors: an analytic model and test results. *Proceedings of ISES Solar World Congress 1991*, Elsevier Science, Vol. 2, Part 1, pp. 1245–1250.
- Kutscher C. F., Christensen C. and Barker G. (1993) Unglazed transpired solar collectors: heat loss theory. *ASME J. Solar Eng.* **115**(3), 182–188.
- Van Decker, G. W. E. (1996) *Asymptotic thermal effectiveness of unglazed transpired plate solar air heaters*, M.A.Sc. Thesis, Department of Mechanical Engineering, University of Waterloo, Canada.
- Zukaurkas A. and Zingzda J. (1985) *Heat Transfer of a Cylinder in Cross Flow*. Hemisphere Publishing Company, New York (ISBN 0-89116-365-4).